Multichannel joint image reconstruction allows for artifact-free focused small field of view magnetic particle imaging

Julia J. Gevaert[1,2], Justin Konkle[3], Patrick Goodwill[3], & Paula J. Foster[1,2]

[1]Cellular and Molecular Imaging Group, Robarts Research Institute, London, ON, Canada
[2]Department of Medical Biophysics, University of Western Ontario, London, ON, Canada
[3]Magnetic Insight Inc., Alameda, CA, United States

Corresponding Author:
Julia J. Gevaert
Department of Medical Biophysics
Robarts Research Institute
University of Western Ontario
1151 Richmond Street North
London, Ontario N6A 5B7
email: jgevaert@uwo.ca

Abstract

Magnetic Particle Imaging (MPI) directly detects superparamagnetic iron oxide (SPIO) labeled cells. We have used MPI to detect SPIO-labeled dendritic cells (DC) migrated to the popliteal lymph nodes (pLN) after injection into the hind footpads. However, in some cases the low pLN signal could not be resolved from nearby higher footpad signal where window leveling to pLN signal oversaturated the footpad signal. The same limitation occurs when SPIO is injected intravenously, accumulates in the liver, and prevents isolation of regions of interest with lower signals. Previous studies have reported on the issue of resolving a wide range of differing iron concentration. A small focused field of view (FOV), to exclude high sources of nearby signal cannot be performed with the standard reconstruction algorithm equipped on the MomentumTM MPI scanner because it is assumed that there is no signal at the edge of the FOV and these values are set to zero for each line along the transmit axis. However, when there is signal at the FOV edge, an inverted negative artifact is created. The multichannel joint reconstruction method uses an iterative reconstruction technique to recover edge information using information from an orthogonal axis, preventing this artifact and allowing the user to prescribe a small FOV on the region of interest. Here we describe the implementation of this method to isolate and quantify low regions of MPI signal from higher regions.

Introduction

First described in 2005[1], magnetic particle imaging (MPI) has recently emerged as a pre-clinical small animal alternative to MRI for cell tracking[2–5]. MPI directly detects the nonlinear magnetization of superparamagnetic iron oxide (SPIO) particles as a signal hot-spot, as opposed to MRI which indirectly detects SPIO as regions of signal loss from its effect on proton relaxation. MPI SPIO signal is quantifiable as it is linearly proportional to iron mass and because ambiguous tissue/bone hypo-intensities that complicate MRI are non-existent with MPI[6]. One of the challenges with implementing MPI for cell tracking studies, is the limited effective dynamic range when there are two or more signals of interest with varying signal intensities within the same imaging field of view (FOV)[7–10]. As a result of this, signal intensity from a higher iron concentration is much larger and overshadows signal coming from a lower iron concentration, preventing detection and subsequently quantification. In a previous study by our group, we used a dendritic cell migration model to quantify lymph-node migrated, SPIO-labeled dendritic cells with MPI but were challenged by this issue. In that model, very high signal from SPIO-labeled dendritic

cells at the injection site, in the mouse footpads, overshadowed nearby lower signal from migrated dendritic cells in the popliteal lymph nodes and prevented quantification in 50% of the nodes[7].

In this study, we explored the use of a small, focused FOV with a multichannel joint image reconstruction algorithm to isolate and quantify MPI signal. This reconstruction was introduced in 2015 by Konkle et al. and uses robust a priori information, non-negativity and image smoothness, to improve image quality[11]. We used an *in vitro* model where a very high signal is approximately 2 cm away from a much lower signal, comparable to our dendritic cell migration model where a bolus of cells is injected intradermally to the mouse footpad and a small percentage of cells (< 5 %) are expected to migrate to the popliteal lymph node. In general, this model could be applied to various pre-clinical scenarios where tracer concentrations can vary over several orders of magnitude within a small area of interest.

Methods

Idealized Dynamic Range – Single Sample – Full FOV

All experiments were performed using the Momentum™ pre-clinical MPI scanner (Magnetic Insight Inc.). The Momentum scanner is a field free line (FFL) scanner that uses a 45 kHz alternating magnetic field to excite SPIO particles and reconstructs images using x-space signal processing[12]. Synomag-D (Micromod GmbH, Germany) was the SPIO used for all experiments. Synomag-D is a multicore particle with a nanoflower substructure. The agglomerated iron core size is ~30 nm, coated with dextran to improve stability and provide compatibility. The resulting hydrodynamic diameter is ~50 nm.

The idealized dynamic range of the MPI system was tested by measuring samples of different concentrations individually. A 1:1 dilution series was prepared using known amounts of Synomag-D, ranging from 50.0 µg Fe to 24.4 ng Fe in 5 µL phosphate buffer solution (PBS) as the highest and lowest iron contents, respectively, for a total of 12 samples (Table 1).

Samples were individually imaged using a 6 x 6 x 12 cm (X, Y, Z) FOV with each sample placed central to the imaging FOV. Projection images were acquired in 2D with a 3.0 T/m selection field gradient and drive field strengths of 20 mT and 23 mT in the X and Z axes, respectively, with an acquisition time of ~2 minutes. These 12 cm FOV images were reconstructed using a native image

reconstruction (the standard reconstruction method for the Momentum™ scanner) enabled by the Regular User Interface (RUI) of the MPI system.

Table 1: Sample preparation for dynamic range experiments.

Sample	S1	S2	S3	S4	S5	S6
Iron (Fe – µg)	50.0	25.0	12.5	6.25	3.13	1.56
Sample	S7	S8	S9	S10	S11	S12
Iron (Fe – ng)	780	391	195	97.7	48.8	24.4

Effective Dynamic Range – Two Samples - Full FOV

The effective dynamic range of the system was tested by measuring samples with different concentrations together within the same 12 cm FOV. In this experiment, S1 (50.0 µg Fe) was placed 2 cm apart from samples with decreasing iron concentrations (S2, S3, S4, etc.) (Figure 2A-H).

Effective Dynamic Range with Distance – Two Samples - Full FOV

Next, the minimum distance required to accurately quantify the highest non-detectable signal (S7, 780 ng Fe) based on the effective dynamic range was tested by increasing its distance from S1 (50.0 µg Fe) incrementally by 1 cm, up to 5 cm, until S7 could be resolved and quantified (Figure 3). Signal profiles were made for each image by plotting a line across the entire image FOV measuring signal intensity.

Two Samples – Small FOV with multichannel joint image reconstruction

In this experiment, S7 (780 ng Fe) sample was placed 2 cm apart from S1 (50 µg Fe) and MPI was repeated with triplicate samples. A 2 cm FOV was centred on S7 and images were acquired for each sample (n = 3) using the standard native reconstruction algorithm used for full 12 cm FOV imaging, and an optimized multi-channel joint reconstruction algorithm which uses an inverse combiner to prevent image artifacts arising from MPI signal detected at the FOV edges, with signal collected along the Z axis[11].

MPI Analysis and Quantification

All MPI images were imported into Horos™, an open-source clinically relevant image analysis software (version 3.3.6, Annapolis, MD USA). Images were viewed using a custom MPI colour look-up table (CLUT). To account for the background signal of the MPI system, an image was acquired of only the sample holder for each image FOV. A region of interest (ROI) encompassing the entire background image was used to determine the standard deviation of the background noise. A threshold value of 5 times the standard deviation of the background noise was applied for subsequent image analysis to ensure only signal above this limit was measured. We have studied various image analysis methods for MPI and found the threshold method to produce accurate quantification with low user variability[13]. Using this threshold, a semi-automatic segmentation tool was used to measure the mean MPI signal within a specific ROI. Total MPI signal for an ROI was calculated by multiplying the ROI area by the mean signal. Calibration lines were made from the 12 and 2 cm (Z) FOV images to show the relationship between iron mass and total MPI signal. These calibration lines were subsequently applied to quantify iron mass from images, respective of FOV. Iron mass was calculated by dividing the total MPI signal by the slope of the respective calibration line for those image parameters. All quantified iron mass was compared to known values provided by the manufacturer. All MPI images were segmented and analyzed in the same way to ensure consistency.

Statistical Methods

A simple linear regression was used to determine the relationship between iron mass and total MPI signal for the 2 cm and 12 cm calibration lines, used for subsequent iron quantification from measured total MPI signal in images. Deviations greater than 10% from known iron values were not considered accurate. For the effective dynamic range experiment (two samples, small FOV) an average of the iron mass estimated from triplicate measurements of S7 was used to compare to the known iron mass using a one sample t and Wilcoxon test.

Results

Idealized Dynamic Range – Single Sample - Full FOV

The idealized dynamic range describes the range of detectable signal from varying iron concentrations when there is only one source of signal within the imaging FOV. Individually imaged samples were detected and quantified from 50 µg Fe (S1) to as low as 48.8 ng Fe (S11) with the chosen parameters. At the next lowest sample (S12, 24.4 ng Fe), the MPI signal was not higher than the threshold limit (5 times the standard deviation of the background signal) and was not considered quantifiable (Figure 1a). In the S12 image, "ghost" signal is observed in the background which is in the same range as the low iron sample[8]. From the S1-S11 images, a calibration line relating MPI signal and iron mass was made and analyzed using a simple linear regression model. There was a strong correlation ($R^2 > 0.9$) between MPI signal and iron mass. The slope of the calibration line was used for quantifying samples in subsequent effective dynamic range experiments (Figure 1b).

The lower bound of the idealized dynamic range was determined by considering the detection of S1-S11 but not S12, representing a dilution factor of $2^{10} = 1024$. The upper bound was not tested beyond S1 (50 µg Fe), since iron concentrations above this amount approached system saturation levels based on MPI relaxometry testing. At very high iron concentrations, the interactions between iron particles tend towards non-linear relations between the particle concentration and the generated signal[14].

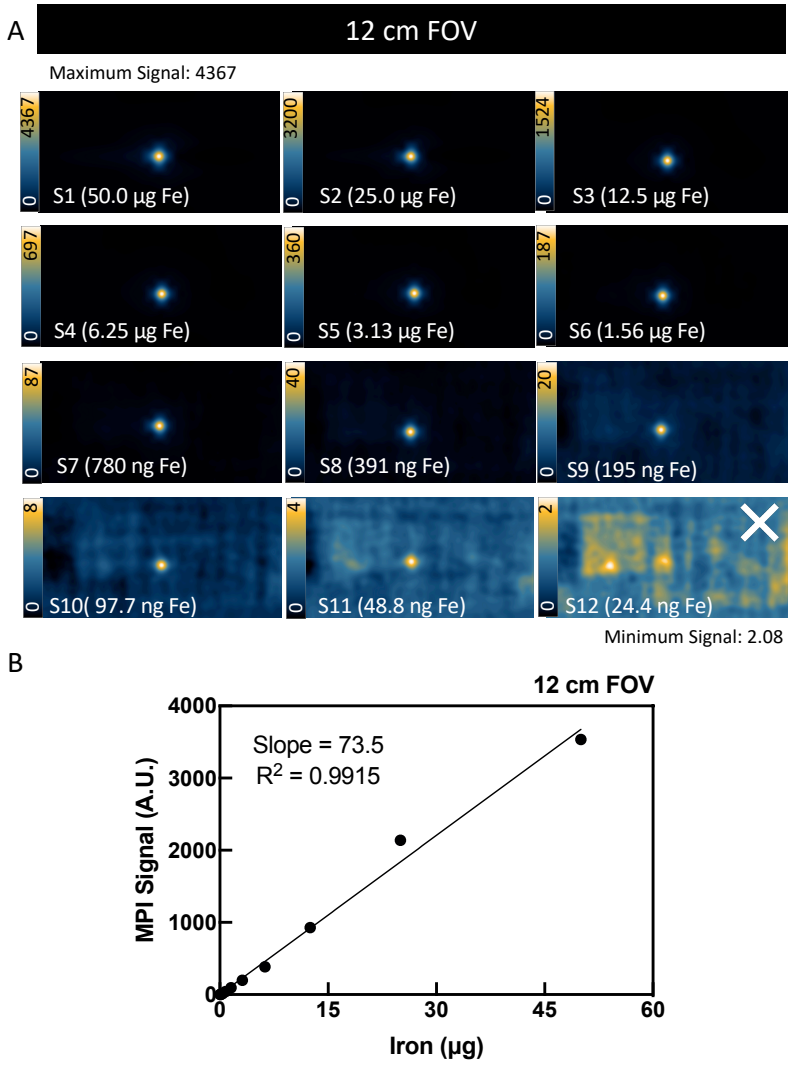

Figure 1: MPI idealized dynamic range for single samples and a full 12 cm FOV. (a) Individually imaged samples were detected and quantified until sample 11 (S11, 48.8 ng Fe) as the detection threshold. (b) Samples 1-11 were quantified and related to MPI signal, showing a strong linear correlation ($R^2 > 0.9$), creating a calibration line used for downstream quantification. The signal from S12 was not detectable and was not quantified, indicated by the white X.

Effective Dynamic Range – Two Samples - Full FOV

The effective dynamic range describes the range of detectable signal when there are two or more signals of varying concentrations within the imaging FOV. In these experiments, a 2-sample model was used where a sample containing a high iron concentration (S1, 50 µg Fe) was placed 2 cm apart from a sample with a lower iron concentration (S2 – S7). Quantification of S1 was consistently within 10% of manufacturer reported values and considered accurate for effective dynamic range experiments. The two samples were imaged with a 12 cm FOV which encompassed both samples. At a 2 cm separation distance, the lower signals from S2-6 were resolved from the higher signal from S1, representing a detection limit of $2^6 = 64$. This limit describes the point at which the lower signal could be resolved from the higher signal using the described threshold method and quantified, though it does not account for accuracy of quantification. Quantification of S6 was considered inaccurate based on our definition of a deviation greater than 10% from known iron values. Therefore, the quantification limit was $2^5 = 32$ (Figure 2). At this limit, with window levels set to the minimum and maximum value of the lower signal, image artifacts begin to appear and become more exaggerated as the iron concentrations decrease. The oversaturated higher signal extends towards the edge of the field of view, resulting in large inverted negative signal artifacts central to the image, affecting low signal isolation and quantification.

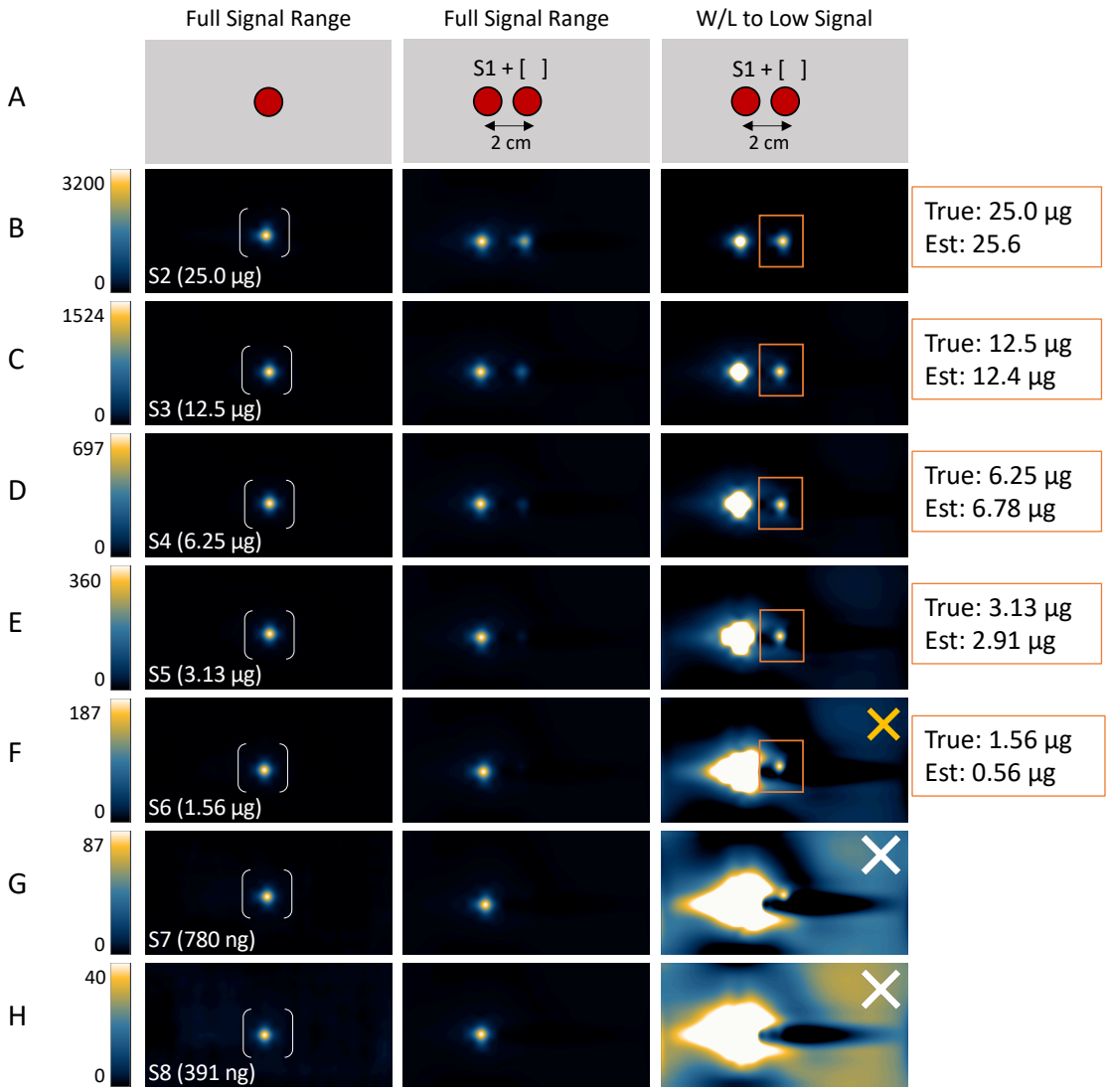

Figure 2: MPI effective dynamic range using two samples of varying iron mass at 2 cm separation imaged with a full 12 cm FOV. Here, the dynamic range of the system is limited to sample 6 (S6, 1.56 µg Fe), a much higher threshold than the idealized range from single sample imaging. Quantification begins to deviate more than 10% with S6. At the next lowest iron mass, S7, the signal cannot be distinguishably quantified from the much higher signal coming from S1 (50.0 µg Fe). In (f), the yellow X indicates signal that was detected but not accurately quantified. The white X in (g) and (h) indicates signal that was not detectable or quantifiable. True means iron mass from manufacturer reported values. Est. means estimated iron mass calculated from calibration lines.

Effective Dynamic Range with Distance – Two Samples - Full FOV

The effective dynamic range significantly changes the limit at which the MPI system can resolve and quantify two varying signals. As a single sample, the system could detect and quantify well below S7 (780 ng Fe), however, when imaged 2 cm apart from S1, a much higher signal, the system could not resolve the lower signal from S7 and prevented quantification. To overcome this effective dynamic range limit at a distance of 2 cm, S7 was placed at increasing separations from the higher S1 sample at 3, 4, and 5 cm (Figure 3). After window leveling to the minimum and maximum signal values for S7, the same image artifacts from the oversaturated high signal are visible, resulting in an inverted negative signal artifact with native image reconstruction. The associated signal profiles are shown adjacent to images. The tall, sharp peak corresponds to the signal coming from S1. At a distance of 2 cm, a smaller peak corresponding to the signal coming from S7 is seen off the shoulder of the larger peak (Figure 3a). The smaller peak shifts to the right of the large peak as separation between the samples increases (Figure 3b, c) until full signal separation and quantification at a distance of 5 cm (Figure 3d). Quantification of S7 was not achieved until a separation distance of 5 cm (Figure 3d). At this distance, the lower signal from S7 was resolved. Using the 12 cm FOV calibration line, S7 was estimated to have 710 ng Fe which was within the 10% accuracy range of the known value, 780 ng Fe (Figure 3).

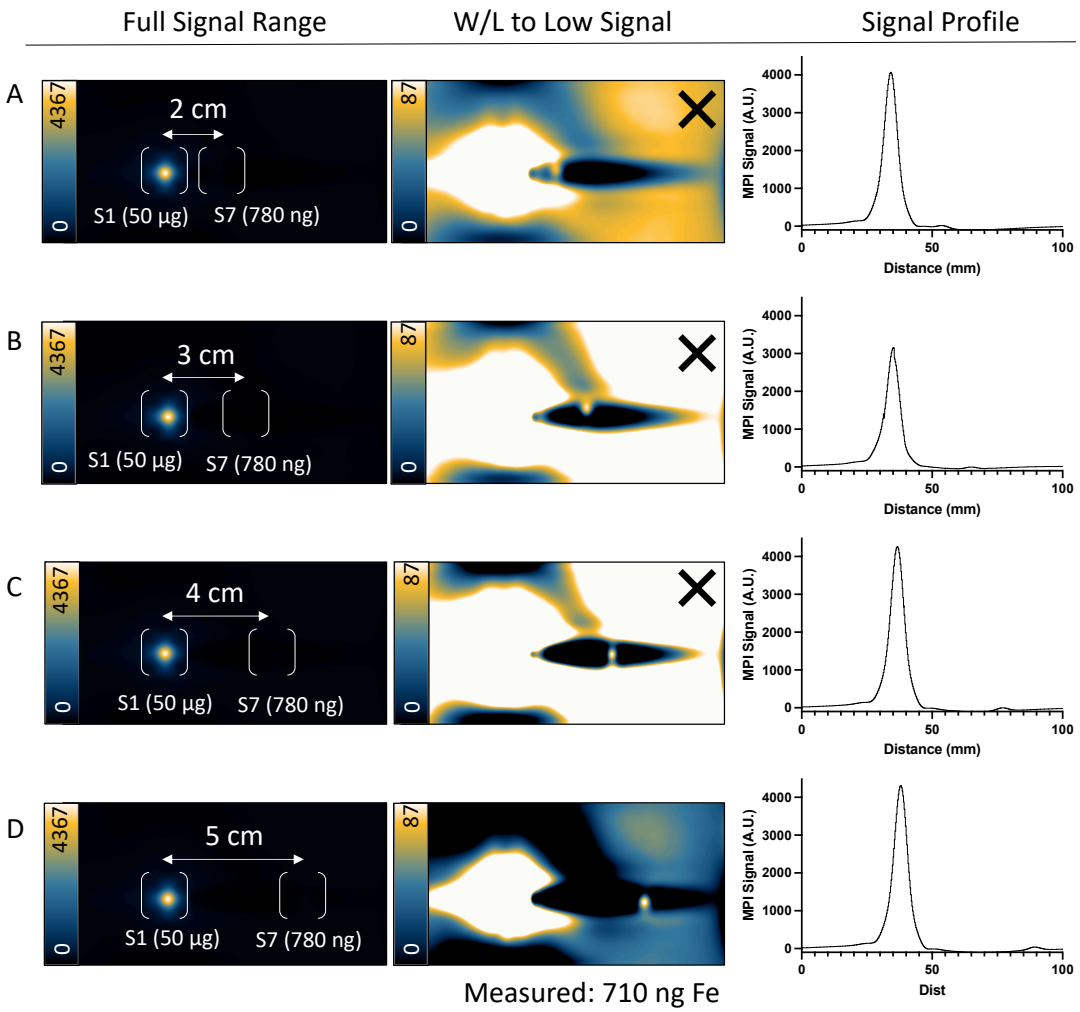

Figure 3: MPI effective dynamic range with increasing distance between two samples imaged within a full 12 cm FOV. Associated signal profiles are shown adjacent to images. The lower signal from sample 7 (S7, 780 ng Fe) could not be resolved or quantified from the higher signal (S1, 50.0 µg Fe) separated by (a) 2 cm, where the signal profile shows a small a small peak (S7) off the shoulder of the large peak (S1). The small peak begins to shift to the left at increasing distances of (c) 3 cm and (d) 4 cm but is not detected or quantified (indicated by the X). To resolve and quantify the lower signal from S7, a minimum distance of 5 cm was required.

Two Samples – Small FOV with multichannel joint image reconstruction

The purpose of this experiment was to investigate using a small, focused FOV to isolate and quantify proximal high and low signals. The same set-up as Figure 3 was used with a 2 cm separation distance between samples. S1 (50 µg Fe) was placed 2 cm apart from S7 (780 ng Fe) and imaged within a 12 cm FOV and native reconstruction (Figure 4a). With the image shown in its full dynamic range (the minimum and maximum signal within the entire FOV), S1 has visible signal but S7 does not (Figure 4b – the same as Figure 3a, first image panel). Window leveling to the minimum and maximum signal of S7 resulted in oversaturation of the higher S1 signal, creating an inverted negative artifact and preventing quantification of the lower S7 signal (Figure 4c – the same as Figure 3a, second image panel). Using the same sample placement, a 2 cm FOV was centered on S7 (Figure 4d). Images were acquired using native reconstruction (Figure 4e) and multi-channel joint reconstruction (Figure 4f). Native reconstruction did not isolate S7 signal or resolve the image artifact which appeared as a negative signal. Native reconstruction automatically assumes there is no signal at the FOV edges and always sets these values to zero. This assumption causes an inverted negative signal artifact to appear on images when there is signal on the FOV edges that is not taken into reconstruction and is automatically set to zero. With this artifact present, quantification was not possible. Multi-channel joint reconstruction fully isolated the low signal within a 2 cm FOV with no image artifacts. Triplicates of S7 (780 ng Fe) were imaged this way with an average iron content of 797 ng Fe estimated from the calibration line. Estimated iron values for the triplicate samples were within 10% of the true value and there was no statistically significant difference between the estimated and true iron values ($p > 0.05$) (Figure 4g).

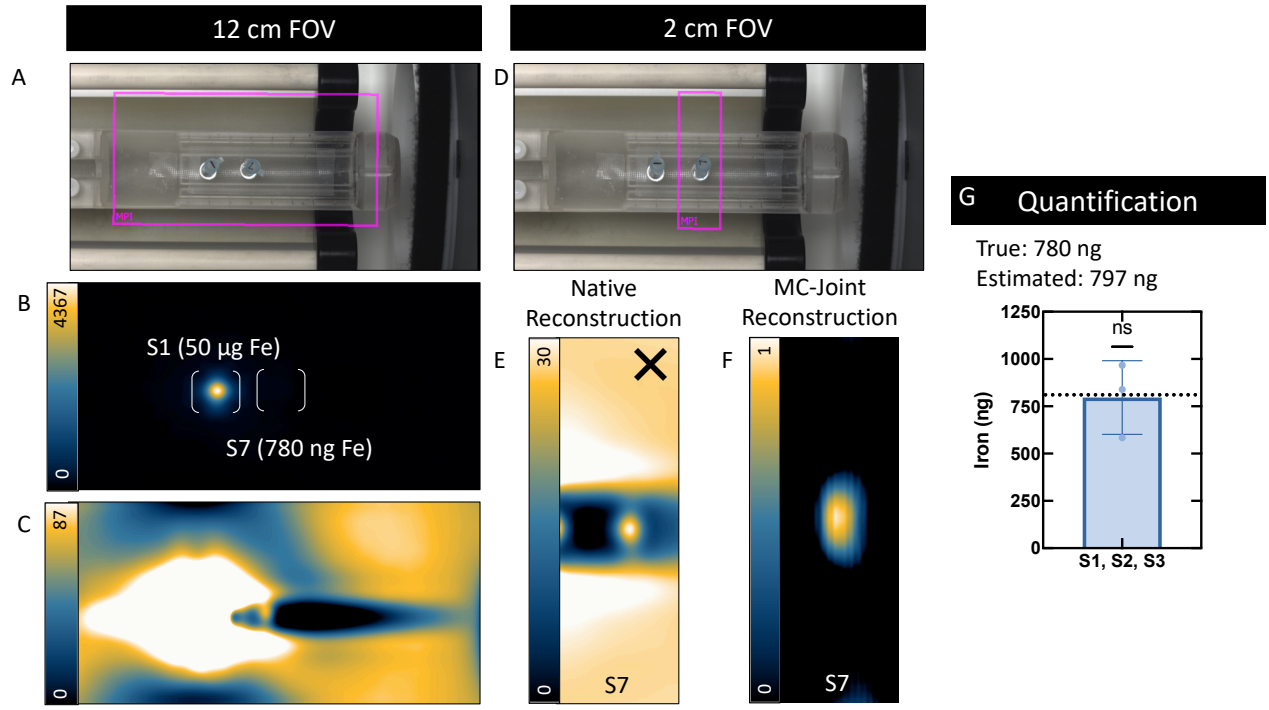

Figure 4: Small field of view (FOV) imaging with multichannel joint reconstruction as a solution to quantifying two proximal samples with varying iron mass. (a) Experimental set-up showing the full 12 cm FOV around a source of low signal (S7, 780 ng Fe) 2 cm apart from a higher signal (S1, 50 µg Fe). (b) Viewing the image in its full dynamic range only shows signal coming from the higher iron sample (S1). (c) Window leveling to the minimum and maximum signal of the lower signal (S7) oversaturates the high signal and prevents quantification of S7. (d) A 2 cm FOV was centred on the low sample (S7) and acquired with (e) native reconstruction, which did not quantify signal (indicated by the X) and (f) multi-channel (MC)- joint reconstruction, which did quantify signal. (g) The MC-joint reconstruction successfully isolated the low signal and triplicate samples were imaged with the average iron content estimated to be 797 ng Fe, in agreement with the known iron content (780 ng Fe) ($p > 0.05$).

Discussion

Our group, and others, have been challenged by resolving proximal high and low MPI signals[7,15]. This is challenging for pre-clinical cell tracking experiments in animal models where a bolus of a high number of SPIO labeled cells is initially injected, and a small percentage of the cells are expected to migrate to different areas of the body. For example, we have studied a dendritic cell (DC) immunotherapy model where a large number of SPIO-labeled DC are injected into the footpads of mice and imaged 48 hours later when a small percentage of DC have migrated to the popliteal lymph nodes. It is generally reported that fewer than 5% of in-vitro DC reach secondary lymphoid tissues[16–20]. This model results in a very high signal in the footpads from remaining non-migratory cells and a very low signal in the popliteal lymph nodes approximately 2 cm away. MPI signal is processed as a "hot spot" where the signal is spread out as a point spread distribution. When two signals are close to each other, their signal distributions may coalesce and prevent signal separation. This is detrimental to signal quantification since ideally, only signals from the area of interest should only be included for quantification. To optimize cell tracking with MPI, this study describes the use of an image reconstruction algorithm that allows for the choice of a small focused FOV to detect and quantify SPIO signal despite its proximity to a higher source of SPIO signal.

Comparing the results from the dilution series of a single sample (Figure 1) with the dilution series of two samples (Figure 2) shows the reduced dynamic range of the MPI system. In the experiments for determining the dynamic range using two samples (high iron mass + low iron mass), to visualize and quantify the lower iron concentrations, the window level had to be adjusted to the minimum and maximum signal of the lower signal; this also put the higher iron concentration within this window level, oversaturating the signal. The lower iron concentrations were quantified until S7 (780 ng Fe), at which point the lower signal could not be isolated from S1 (50.0 µg Fe). In these experiments, within a full 12 cm FOV, the native reconstruction algorithm could resolve a dynamic range of about $2^5 = 32$ for a distance of 2 cm. In Figure 5, we explored the use of a 2 cm focused small FOV centered on the low iron mass sample as a solution to the challenge of isolating weaker signal from the dominating higher signal. With the small FOV, a multi-channel joint reconstruction algorithm[11] was used that produced an artifact-free image of the low iron sample without impeding signal from the higher sample. This dynamic range issue has been explored by others[8–10]. Boberg et al proposed a two-step reconstruction algorithm which increased

the dynamic range and reduced image artifacts by separating the total signal into two constituents; high and low, and using different thresholds for their respective reconstruction. Graeser et al also proposed a type of reconstruction improvement which combined suppressing the excitation signal at its base frequency via a band-stop filter and recovering the particle signal by compensating the excitation signal in the receive chain. Optimized image reconstruction is being demonstrated as a solution to low signal isolation; however, on commercially available systems this may be challenging when implementation and accessibility would come from the manufacturer.

Previously, the use of a focused small field of view (FOV) to isolate low signal regions was challenging, if not impossible, with the prescribed native reconstruction algorithm equipped on the Momentum™ MPI scanner as the only reconstruction option available. The regular native image reconstruction algorithm assumed that there is no signal along the edges of the FOV; if there was signal present, the values were set to zero for each line along the transmit axis[11,12]. This assumption caused an inverted negative image artifact when there was signal present at the FOV edge which prevented signal detection and quantification if the assumptions were not met.

Small FOV imaging with MPI on the Momentum scanner is early in its development. For this experiment, our MPI system was upgraded to allow the user access to an advanced user interface where image sequences could be changed through the configuration editor. Most importantly, this permitted the use of a novel reconstruction algorithm referred to as multi-channel joint image reconstruction[11] recently implemented as a reconstruction option on the Momentum™ scanner. The multichannel joint reconstruction method uses an iterative reconstruction technique to recover edge information using information from an orthogonal axis, preventing the negative inverted signal artifact and allowing the user to prescribe a small FOV without concern for whether signal is present at the FOV edge. This study demonstrates the feasibility of using this type of reconstruction to resolve and quantify discrete sources of signal with reduced interference from large, proximate iron concentrations which are not of interest. Additionally, using a focused small FOV reduced image acquisition time by 50%.

References

1. Gleich, B. & Weizenecker, J. Tomographic imaging using the nonlinear response of magnetic particles. *Nature* **435**, 1214–1217 (2005).
2. Tay, Z. W. *et al.* In vivo tracking and quantification of inhaled aerosol using magnetic particle imaging towards inhaled therapeutic monitoring. *Theranostics* **8**, 3676–3687 (2018).
3. Sedlacik, J. *et al.* Magnetic Particle Imaging for High Temporal Resolution Assessment of Aneurysm Hemodynamics. *PLoS One* **11**, e0160097 (2016).
4. Zheng, B. *et al.* Quantitative Magnetic Particle Imaging Monitors the Transplantation, Biodistribution, and Clearance of Stem Cells In Vivo. *Theranostics* **6**, 291–301 (2016).
5. Arami, H. *et al.* Tomographic magnetic particle imaging of cancer targeted nanoparticles. *Nanoscale* **9**, 18723–18730 (2017).
6. Paysen, H. *et al.* Cellular uptake of magnetic nanoparticles imaged and quantified by magnetic particle imaging. *Scientific Reports* **10**, 1922 (2020).
7. Gevaert, J. J., Fink, C., Dikeakos, J. D., Dekaban, G. A. & Foster, P. J. Magnetic Particle Imaging Is a Sensitive In Vivo Imaging Modality for the Detection of Dendritic Cell Migration. *Mol Imaging Biol* (2022) doi:10.1007/s11307-022-01738-w.
8. Boberg, M. *et al.* Simultaneous imaging of widely differing particle concentrations in MPI: problem statement and algorithmic proposal for improvement. *Phys. Med. Biol.* **66**, 095004 (2021).
9. Herz, S. *et al.* Selective Signal Suppression in Traveling Wave MPI: Focusing on Areas with Low Concentration of Magnetic Particles. *International Journal on Magnetic Particle Imaging* **3**, (2017).

10. Franke, J. *et al.* System Characterization of a Highly Integrated Preclinical Hybrid MPI-MRI Scanner. *IEEE Transactions on Medical Imaging* **35**, 1993–2004 (2016).
11. Konkle, J. J. *et al.* A Convex Formulation for Magnetic Particle Imaging X-Space Reconstruction. *PLOS ONE* **10**, e0140137 (2015).
12. Goodwill, P. W., Konkle, J. J., Zheng, B., Saritas, E. U. & Conolly, S. M. Projection X-Space Magnetic Particle Imaging. *IEEE Trans Med Imaging* **31**, 1076–1085 (2012).
13. Sehl, O. C. *et al.* MPI region of interest (ROI) analysis and quantification of iron in different volumes. *International Journal on Magnetic Particle Imaging* **8**, (2022).
14. Loewa, N., Radon, P., Kosch, O. & Wiekhorst, F. Concentration Dependent MPI Tracer Performance. *International Journal on Magnetic Particle Imaging* **Vol.2**, 5 pages (2016).
15. Makela, A. V. *et al.* Magnetic Particle Imaging of Macrophages Associated with Cancer: Filling the Voids Left by Iron-Based Magnetic Resonance Imaging. *Mol Imaging Biol* **22**, 958–968 (2020).
16. De Vries, I. J. M. *et al.* Effective migration of antigen-pulsed dendritic cells to lymph nodes in melanoma patients is determined by their maturation state. *Cancer Res* **63**, 12–17 (2003).
17. Eggert, A. A. O. *et al.* Biodistribution and Vaccine Efficiency of Murine Dendritic Cells Are Dependent on the Route of Administration. *Cancer Res* **59**, 3340–3345 (1999).
18. Eggert, A. A. O. *et al.* Analysis of dendritic cell trafficking using EGFP-transgenic mice. *Immunol Lett* **89**, 17–24 (2003).
19. Josien, R. *et al.* Trance, a Tumor Necrosis Factor Family Member, Enhances the Longevity and Adjuvant Properties of Dendritic Cells in Vivo. *J Exp Med* **191**, 495–502 (2000).
20. MartIn-Fontecha, A. *et al.* Regulation of dendritic cell migration to the draining lymph node: impact on T lymphocyte traffic and priming. *J Exp Med* **198**, 615–621 (2003).

21. Harvell-Smith, S., Tung, L. D. & Thanh, N. T. K. Magnetic particle imaging: tracer development and the biomedical applications of a radiation-free, sensitive, and quantitative imaging modality. *Nanoscale* **14**, 3658–3697 (2022).
22. Fink, C. *et al.* Fluorine-19 Cellular MRI Detection of In Vivo Dendritic Cell Migration and Subsequent Induction of Tumor Antigen-Specific Immunotherapeutic Response. *Mol Imaging Biol* **22**, 549–561 (2020).
23. Fink, C. *et al.* 19F-perfluorocarbon-labeled human peripheral blood mononuclear cells can be detected in vivo using clinical MRI parameters in a therapeutic cell setting. *Sci Rep* **8**, 590 (2018).
24. Fink, C. *et al.* Quantification and characterization of granulocyte macrophage colony-stimulating factor activated human peripheral blood mononuclear cells by fluorine-19 cellular MRI in an immunocompromised mouse model. *Diagnostic and Interventional Imaging* **101**, 577–588 (2020).